ACS APPLIED ENERGY MATERIALS

www.acsaem.org
Article

Cosintering the Anode Active Material with $Li_7La_3Zr_2O_{12}$ Solid Electrolyte for the All-Solid-State Battery: How to Predict the Interfacial Reaction at Elevated Temperatures

Zongqi He, Ken Watanabe,* Koichi Suematsu, Kazutaka Mitsuishi, and Kengo Shimanoe

Cite This: ACS Appl. Energy Mater. 2025, 8, 16964−16973
Read Online

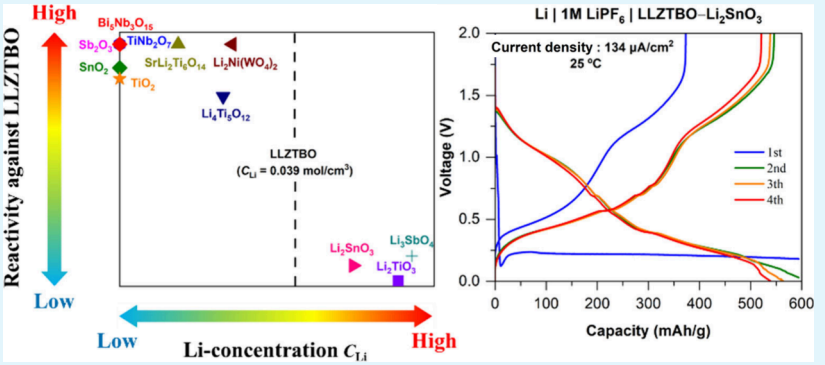

ABSTRACT: Cosintered-type all-solid-state batteries composed of $Li_7La_3Zr_2O_{12}$ (LLZ) have garnered significant attention as next-generation batteries that offer both high energy density and long cycle life. However, achieving low-resistance interfaces through cosintering of electrode materials, particularly between the anode active material and LLZ, remains a big challenge due to the formation of reaction phases caused by interdiffusion during high-temperature sintering. In this study, we demonstrated the lithium concentration within the materials (C_{Li}: mol/cm^3) as a key factor for predicting the reactivity between the anode active material and LLZ during high-temperature sintering. Various kinds of anode active materials with different C_{Li} values were mixed with LLZ, and the reactivity during sintering at 850 °C was carefully investigated. XRD results show that interfacial reaction proceeds between LLZ and low C_{Li} materials due to the occurrence of Li loss in LLZ. Contrarily, Li_2SnO_3, Li_2TiO_3, and Li_3SbO_4 in the high C_{Li} group (larger than that of LLZ) achieve interaction suppression against the LLZ electrolyte during high-temperature sintering. However, lattice parameter characterization and TEM images reveal that interdiffusion and side reactions occurred at the interface layer in the composite LLZ/high C_{Li} material. Densified composite LLZTBO−Li_2SnO_3 (relative density ∼ 89%) and LLZTBO−Li_2TiO_3 pellets (∼95%) were successfully obtained under 900 °C sintering for 15 h. Charge−discharge tests using the half-cell assembled with the cosintered composite anode and liquid electrolyte reveal the superior capacity of 550 mAh/g with nearly 92% Coulombic efficiency for the LLZTBO−Li_2SnO_3 cosintered anode. The approach reported herein has the potential to rapidly screen possible cosintered electrodes for garnet-type solid-state electrolytes and achieve cosintered-type all-solid-state batteries with high energy density.

KEYWORDS: *Anode, Garnet-type LLZ, Cosintered, All-solid-state, Lithium battery*

1. INTRODUCTION

In recent years, lithium-ion batteries (LiBs) have been regarded as the most widely used energy storage system (ESS) in several fields, including electric vehicles (EVs), isolated energy storage devices, and portable devices such as smartphones and laptops.[1] However, with the development of advanced rechargeable batteries, LiBs have faced several critical issues regarding energy density and safety. The incompatibility between the liquid electrolyte and highly advanced cathode and anode materials limits LiBs from meeting the future needs of rechargeable batteries. Moreover, the flammability of liquid LiBs also poses a safety hazard.[2−5]

Solid-state electrolytes (SSEs) are considered good alternatives to conventional batteries based on liquid electrolytes due to their advantages, including a wide electrochemical window, strong mechanical, thermal, chemical, and electrochemical stability, and high ionic conductivity.[6−9] The family of SSEs, including solid polymer electrolytes,[10] inorganic oxide

Received: September 16, 2025
Revised: October 27, 2025
Accepted: October 28, 2025
Published: November 4, 2025

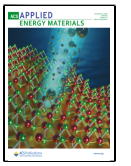

electrolytes,[11−13] inorganic sulfide electrolytes,[14] and others such as metal−organic frameworks,[15] has been widely investigated in recent years. Among them, garnet-type SSEs have emerged as one of the most promising and vital candidates due to their high ionic conductivity (10^{-4}−10^{-3} S/cm), good chemical stability against Li-metal, wide potential window (0−9 V), and negligible electronic transport.[16−19]

In 2007, $Li_7La_3Zr_2O_{12}$ (LLZ), with a high Li-ionic conductivity of 3×10^{-4} S/cm, was successfully prepared for the first time by sintering at 1230 °C for 36 h.[20] Since LLZ garnet-based electrolytes provide significant advantages in ionic conductivity, safety, chemical, thermal, and electrochemical stability, as well as air stability, extensive research has been carried out on the LLZ-based all-solid-state lithium batteries (ASSLBs). LLZ is reported to have tetragonal phases (space group $I4_1/acd$) and cubic phases (space groups $Ia\bar{3}d$ and $I\bar{4}3d$). The conductivity of the cubic phase is more than 2 orders of magnitude higher than that of the tetragonal phase, and it is stable at high temperatures.[21] Therefore, numerous doping strategies have emerged to stabilize the cubic phases at room temperature, including Ga^{3+}, Al^{3+}, or Ge^{3+} doped into the Li-sites[22−27] or Ta^{5+}, Gd^{3+}, Te^{5+}, Mo^{6+}, Ce^{4+}, Nb^{5+}, Sb^{5+}, or Bi^{5+} into the Zr-sites.[28−37] In addition, to obtain dense pellets and high ionic conductivity of LLZ, sintering at a temperature over 1000 °C is essential to reduce grain boundary resistance.[38−43]

For various ASSLBs operations, forming a composite electrode (CE) via mixing an active material and SSE, followed by a cosintering process, is a suitable approach to lower the interfacial resistance and facilitate fast Li-ion transportation by providing a continuous pathway. Hence, the electrochemical and chemical interactions between LLZ and an electrode material should be considered to be significant factors. High-temperature sintering may form a highly resistive interface phase due to interdiffusion and unexpected reactions between the LLZ and the electrode material, resulting in poor battery performance.

To prevent the interfacial reaction caused by sintering at high temperatures above 1000 °C, it is crucial to lower the sintering temperature to a range stable for coexisting SSEs and active materials thermodynamically.[44,45] In recent years, various cathode materials, such as $LiCoO_2$,[46] have been investigated for use in a cosintering type of cathode with a solid-state electrolyte. Our group has reported that Bi substitution and composition control can significantly reduce the sintering temperature of LLZ, allowing it to be cosintered with $LiCoO_2$.[47−50] However, there are still few reports on viable anode materials for LLZ, and the selection of anode materials applicable to LLZ-based ASSLBs has yet to progress. To date, the most widely used anode for an LLZ-based electrolyte is Li-metal. Although Li-metal exhibits ultrahigh specific capacity (3860 mAh/g) and a large negative potential of −3.04 V,[51] high interfacial resistance and the growth and expansion of Li dendrites remain significant challenges and are unsolved.[52−55]

In this study, we aimed to explore the anode materials that can be cosintered with the LLZ-based electrolyte. In the case of anode materials, achieving both reaction suppression during sintering and high energy density is essential. Candidates including SnO_2, TiO_2, Sb_2O_3, $TiNb_2O_7$, $Bi_5Nb_3O_{15}$, $SrLi_2Ti_6O_{14}$, $Li_2Ni(WO_4)_2$, Li_2SnO_3, Li_2TiO_3, and Li_3SbO_4 have been chosen. The reaction between varied materials is generally predictable from thermodynamic calculations, because it proceeds when $\Delta G°$ is negative. Moreover, the reaction kinetics determine the progress of the reaction. Chemical potential (μ) difference could be regarded as a significant driving force of interdiffusion. However, calculating the chemical potential of Li for many materials requires significant time and cost. Herein, we attempted to simplify "μ" to "Li-concentration (C_{Li}: mol/cm^3)" in the LLZ/anode cosintered system, because C_{Li} can be easily estimated from crystallographic databases. Therefore, the relationship between C_{Li} of electrode materials and the reactivity of the LLZ was investigated. The information on the C_{Li} of anode candidates is shown in Table 1. Ideally, the electrode materials should not react with LLZ at elevated temperatures and should also be densified simultaneously to create a suitable interface for Li-ion conduction. Thus, in this study, to justify suitable materials for cosintering with LLZ, the crystal structure change and sintering properties were investigated in detail.

Table 1. Lithium Concentration of Anode Candidates and SSEs

Material	Li-concentration C_{Li} [mol/cm^3]
SnO_2	0
TiO_2	0
Sb_2O_3	0
$TiNb_2O_7$	0
$Bi_5Nb_3O_{15}$	0
$SrLi_2Ti_6O_{14}$	0.014
$Li_2Ni(WO_4)_2$	0.025
$Li_4Ti_5O_{12}$	0.030
$Li_{6.5}La_3Zr_{1.5}Ta_{0.3}Bi_{0.2}O_{12}$(LLZTBO)	**0.039**
Li_2SnO_3	0.055
Li_2TiO_3	0.062
Li_3SbO_4	0.065

2. EXPERIMENTAL SECTION

2.1. Synthesis of LLZ-Based Electrolytes. $Li_{6.5}La_3Zr_{1.5}Ta_{0.3}B_{i0.2}O_{12}$ (LLZTBO) compounds were synthesized through a conventional solid-state reaction (SSR). Li_2CO_3 (>99.99%; Rare Metallic Co., Ltd., Japan), $La(OH)_3$ (>99.9%; Sigma-Aldrich, Germany), ZrO_2 (>98%; Kojundo Chemical Laboratory Co., Ltd., Japan), Bi_2O_3 (>98%; Sigma-Aldrich, Germany), and Ta_2O_5 (>99.9%; FUJIFILM Wako Pure Chemical Corporation, Japan) were used as starting materials. 2% excess of Li_2CO_3 and stoichiometric ratio of the remaining starting materials were weighted and mixed by ball-milling in 2-propanol using 3 mm diameter of Tungsten balls for 20 h. After full evaporation of the solvent, the mixtures were ground in 2-propanol for 30 min. The samples were then dried at 105 °C for 2 h and calcined in an alumina crucible at 800 °C for 15 h with a ramp rate of 400 °C/h. After calcination, to obtain a small particle size, the resultant powders were repeatedly ground for 15 min and then ball-milled in 2-propanol for 900 min, and this was repeated 2 times. The resulting samples were then fully dried, ground, and used for further research.

2.2. Synthesis of Anode Candidates. SnO_2 (>99.9%; Kojundo Chemical Laboratory Co., Ltd., Japan), TiO_2 (>99.8%; FUJIFILM Wako Pure Chemical Corporation, Japan), and Sb_2O_3 (>99.9%; FUJIFILM Wako Pure Chemical Corporation, Japan) were directly used as anode candidates. All of the remaining anode candidates, including $Bi_5Nb_3O_{15}$, $TiNb_2O_7$, $SrLi_2Ti_6O_{14}$, $Li_2Ni(WO_4)_2$, Li_2SnO_3, Li_2TiO_3, and Li_3SbO_4, were prepared using a conventional SSR, with weights in stoichiometric ratios with an excess of Li_2CO_3 additive. All the precursor materials were mixed by ball-milling in 2-propanol using zirconia balls of 1 mm diameter for 15 h. After evaporation of the solvent, the mixtures were calcinated and placed on a Au sheet under

https://doi.org/10.1021/acsaem.5c02930
ACS Appl. Energy Mater. 2025, 8, 16964−16973

different conditions. The resultant samples were subsequently ground for 15 min. The information on starting materials, excess of Li source, and calcination conditions are shown in Table S1.

2.3. Preparation of Composite Pellets (CPs). Each anode candidate and LLZTBO were mixed in a weight ratio of 1:1 in 2-propanol through uniaxial ball-milling at 625 rpm for 15 h, separately. After proper mixing, the mixtures were dried and pressed into pellets (0.2 g) through uniaxial pressing under a pressure of 1.5 MPa and subsequent Cold Isostatic Pressing at 360 kgf/cm. Thereafter, those CPs were sintered at 850 °C for 5 h with a ramp rate of 5 °C/min. An Au sheet was placed on the bottom of the pellets to prevent Al contamination from the alumina setter.

2.4. Material Characterization. Crystal structure and phase identification of each CP were conducted by X-ray diffraction (XRD) using a SmartLab device (Rigaku, Japan) with Cu Kα radiation. Element distribution was probed by transmission electron microscopy (TEM) (JEM-ARM200F, JEOL, Japan). Relative densities were calculated from the bulk and theoretical densities. Lattice parameters were refined by Rietveld analysis using PDXL2 software (Rigaku, Japan). Impurity ratio R_i of each anode candidate could be calculated through Equation 1:

$$R_i = \frac{n(Total\ Reflections\ associated\ to\ Impurity\ phases)}{n(All\ diffraction\ peaks)} \times 100\% \quad (1)$$

To reveal the sintering behavior of the composite pellets, typical samples were cosintered at different temperatures for 5 h at a constant heating rate of 5 °C/min.

2.5. Electrical Characterization. The electrode performance of a typical composite LLZ/anode dense electrode was measured through a liquid-electrolyte based half-cell: Lil1 M $LiPF_6$ (EC: DEC = 1:2 (vol %)|composite LLZ/anode. The CPs were polished to a thickness of 200 μm with sandpaper (Grit 600). The Pt film was sputtered on the surface of the CPs as a current collector. A glass microfiber filter (Φ21 mm, Whatman GF/A) was used as a separator. The half-cells were cycled galvanostatically between 0 and 2 V at room temperature by using a battery test system (HJ1020mSD8, Hokuto Denko, Japan).

3. RESULTS AND DISCUSSION

3.1. Relationship between C_{Li} in the Electrode Materials and the Reactivity of LLZTB. Anode active materials, including SnO_2, TiO_2, Sb_2O_3, $TiNb_2O_7$, $Bi_5Nb_3O_{15}$, $SrLi_2Ti_6O_{14}$, and $Li_2Ni(WO_4)_2$, the C_{Li} values of which are smaller than that of LLZTB, are defined as the low C_{Li} group. Contrarily, Li_2SnO_3, Li_2TiO_3, and Li_3SbO_4, the C_{Li} of which are higher than that of LLZ, are classified in the high C_{Li} group. SnO_2 has been widely reported as an anode for lithium batteries.[56] In addition, Li_2SnO_3 has attracted considerable attention as an anode for Li-ion battery due to the theoretical capacity of tin being as high as 993 mAh/g.[57] Herein, SnO_2 (Low C_{Li} group) and Li_2SnO_3 (High C_{Li} group) were presented as a typical comparative group. $TiO_2/Li_4Ti_5O_{12}/Li_2TiO_3$ is an additional comparative group presented below.

XRD patterns of synthesized Li_2SnO_3, composite LLZTBO−SnO_2, and LLZTBO−Li_2SnO_3 pellets are shown in Figure 1. As can be seen, for the LLZTBO−SnO_2 composite pellets, the diffraction peaks of LLZTBO completely disappeared, whereas the presence of Li_2SnO_3, SnO_2, $La_{2.4}Zr_{1.2}Ta_{0.24}Bi_{0.16}O_7$, and unknown impurities could be observed after cosintering at 850 °C for 5 h, indicating an extremely weak chemical stability of LLZTBO against low C_{Li} substance SnO_2. The impurity ratio R_i of SnO_2 is about 90%. Nevertheless, a cosintered LLZTBO−Li_2SnO_3 composite pellet was successfully prepared under the same sintering conditions. As seen in Figure 1, the diffraction peaks of LLZTBO−Li_2SnO_3 could be clearly distinguished as Li_2SnO_3

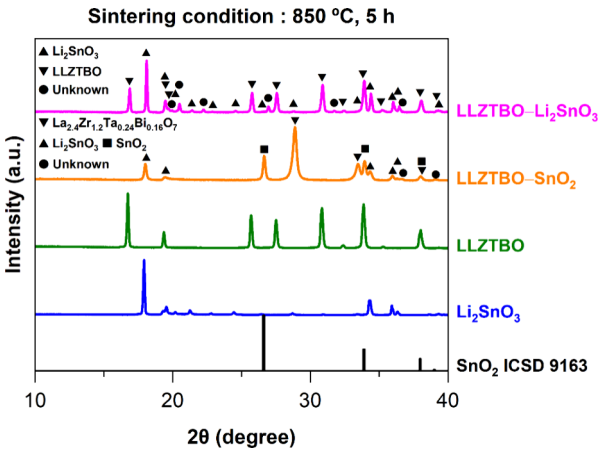

Figure 1. XRD patterns of synthesized Li_2SnO_3, LLZTBO−SnO_2, and LLZTBO−Li_2SnO_3 pellets.

and LLZTBO, while a few unknown impurity phase peaks of 9% appear.

It has been reported that fluorite-type $La_{2.4}Zr_{1.2}Ta_{0.4}O_7$ is a precursor oxide for low-temperature formation of garnet-type $Li_{6.5}La_3Zr_{1.5}Ta_{0.5}O_{12}$.[58] Therefore, in view of the huge difference of C_{Li} between SnO_2 (0 mol/cm^3) and LLZTBO (0.039 mol/cm^3), we could speculate that the diffraction peak of $La_{2.4}Zr_{1.2}Ta_{0.24}Bi_{0.16}O_7$ in Figure 1 is probably derived from the decomposition of LLZTBO due to the drastic C_{Li} difference between SnO_2 and LLZTBO, resulting in Li-ion loss from electrolyte to electrode. The reaction between Li ions and SnO_2 initiated the generation of Li_2SnO_3. Notably, the weight ratio of composite LLZTBO−SnO_2 in the work was set as 1:1, indicating that the molar ratio of LLZTBO and SnO_2 was about 1:5.88. Thus, the chemical reaction between LLZTBO and SnO_2 after cosintering at 850 °C for 5 h could be estimated as below:

$$Li_{6.5}La_3Zr_{1.5}Ta_{0.3}Bi_{0.2}O_{12} + 5.88SnO_2 \rightarrow 1.25La_{2.4}Zr_{1.2}Ta_{0.24}Bi_{0.16}O_7 + 3.25Li_2SnO_3 + 2.63SnO_2$$

Phase identification of the $TiO_2/Li_4Ti_5O_{12}/Li_2TiO_3$ comparative group was conducted and is recorded in Figure 2.

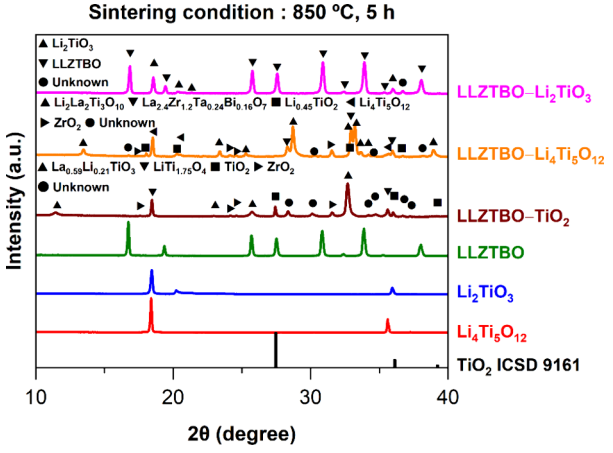

Figure 2. XRD patterns of $Li_4Ti_5O_{12}$, Li_2TiO_3, LLZTBO−TiO_2, LLZTBO−$Li_4Ti_5O_{12}$, and LLZTBO−Li_2TiO_3 pellets.

https://doi.org/10.1021/acsaem.5c02930
ACS Appl. Energy Mater. 2025, 8, 16964−16973

XRD results were consistent with those of SnO_2/Li_2SnO_3. Low reactivity between Li_2TiO_3 in the high C_{Li} group and LLZTBO after cosintering at 850 °C for 5 h could be concluded due to the presence of the diffraction peaks of electrolyte and anode material in the LLZTBO−Li_2TiO_3 composite pellets. Contrarily, no matching of active materials or LLZTBO reflects in LLZTBO−$Li_4Ti_5O_{12}$ as well as LLZTBO−TiO_2 in Figure 2 implies that $Li_4Ti_5O_{12}$ or TiO_2 in the low C_{Li} group completely reacted with LLZTBO after cosintering at 850 °C. Notably, the appearance of $La_{2.4}Zr_{1.2}Ta_{0.24}Bi_{0.16}O_7$ diffraction peak in LLZTBO−$Li_4Ti_5O_{12}$ indicated the decomposition of LLZTBO. Moreover, the appearance of various Li−La−Ti−O compounds reflected the absence of $La_{2.4}Zr_{1.2}Ta_{0.24}Bi_{0.16}O_7$ in the LLZTBO−TiO_2 composite pellets, indicating the subsequent inter-reaction between intermediates and fluorite-type species. Thereafter, XRD results of Sb_2O_3/Li_3SbO_4 comparative group, as well as the rest of the anode candidates in the low C_{Li} group, were conducted (Figures S1−S5). All of the C_{Li} materials reacted with LLZTBO at 850 °C, and LLZTBO disappeared as well.

Based on the above results, the relationship between C_{Li} in the electrode materials and the reactivity with LLZTBO has been summarized in Figure 3. As can be seen, the relationship

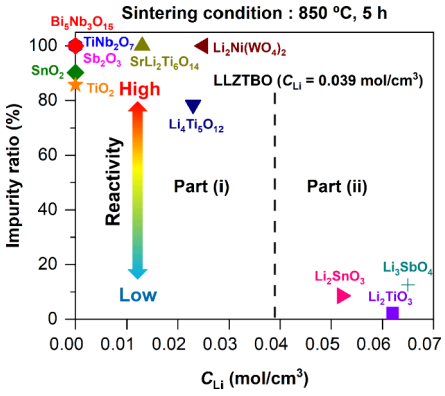

Figure 3. Relationship between C_{Li} in the electrode materials and the reactivity of LLZTBO.

could be divided into two parts: (i) Low C_{Li} group showing high reactivity with LLZTB, and (ii) high C_{Li} group showing low reactivity with LLZTBO. In the case of highly reactive anode candidates in part (i), the huge difference in C_{Li} between anode and LLZTB is a prerequisite of lithium diffusion from electrolyte to electrode during high-temperature sintering, leading to drastic loss of lithium ion in LLZTBO, thus decomposing the LLZTBO crystal structure, and the subsequent chemical interaction occurred between intermediate of LLZTB and anode material. On the other hand, materials with larger C_{Li} than that of LLZTBO in part (ii) exhibit strong chemical stability against LLZTB even at 850 °C. As the driving force of the C_{Li} difference no longer exists, LLZTBO can easily maintain its structure after sintering, leading to the successful preparation of the cosintered composite anode material.

The above results demonstrated that anode candidates in the low C_{Li} group show strong reactivity with LLZTBO. Therefore, the starting reaction temperature could be considered as an index to define the driving force of interaction between LLZTBO and anode candidates with a low C_{Li}. The range of the minimum reaction temperature (T_R) could be easily characterized through XRD results and by sintering at different temperatures. Figure 4(a) and Figure 4(b) show the peak changes of LLZTBO−SnO_2 and LLZTBO−TiO_2 at different temperatures, respectively. In Figure 4(a), the diffraction peaks of LLZTBO and SnO_2 remained after sintering at 650 °C, compared to the pristine composite sample. When the temperature increased to 750 °C, the diffraction peak of LLZTBO disappeared, whereas new peaks of intermediates could be observed. Therefore, the reaction-starting temperature between LLZTBO and SnO_2 was between 650 and 750 °C. Moreover, as seen in Figure 4(b), when sintering at 327 °C, although the XRD pattern matched that of pristine composite samples, the intensity of the LLZTBO peak decreased. As the sintering temperature further increased to 450 °C, the reaction between TiO_2 and LLZTBO proceeded because of the absence of LLZTBO as well as the presence of an intermediate diffraction peak. Thus, the initial reaction temperature of composite LLZTBO−TiO_2 was predicted between 327 and 450 °C.

Furthermore, XRD patterns of the other candidates are shown in the Supporting Information (Figures S6−S11). The range of reaction-starting temperatures of different candidates is summarized in Table 2. Sb_2O_3 exhibited the strongest driving force of interfacial reaction with LLZTBO among all the candidates due to the lowest initial reaction temperature against LLZTBO. The chemical stability of TiO_2, $Bi_5Nb_3O_{15}$, $Li_4Ti_5O_{12}$, and $Li_2Ni(WO_4)_2$ was in the middle class, which was stronger than that of Sb_2O_3. Notably, the interfacial reaction driving forces of $TiNb_2O_7$, $SrLi_2Ti_6O_{14}$, and SnO_2 against LLZTBO were weaker than those of the middle class,

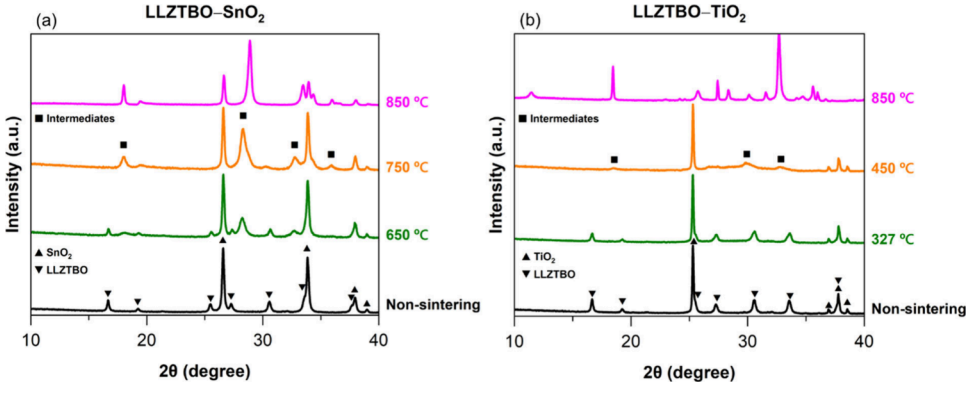

Figure 4. XRD patterns of (a) LLZTBO−SnO_2 and (b) LLZTBO−TiO_2 sintering at different temperatures.

https://doi.org/10.1021/acsaem.5c02930
ACS Appl. Energy Mater. 2025, 8, 16964−16973

Table 2. Range of Starting Reaction Temperature of Cosintered LLZTBO and Low C_{Li} Group Materials

Anode materials	Li-concentration C_{Li} [mol/cm^3]	Range of Min T_R
Sb_2O_3	0	253−333 °C
TiO_2	0	327−450 °C
$Bi_5Nb_3O_{15}$	0	346−450 °C
$Li_4Ti_5O_{12}$	0.030	375−450 °C
$Li_2Ni(WO_4)_2$	0.025	388−450 °C
$TiNb_2O_7$	0	450−550 °C
$SrLi_2Ti_6O_{14}$	0.014	550−650 °C
SnO_2	0	650−750 °C

with the forces decreasing in order. Therefore, among the group of materials with low C_{Li}, no clear correlation was observed between the onset temperature of the reaction with LLZTBO and the C_{Li}. This implied that the reaction onset temperature was governed not by the reaction rate driven by differences in Li concentration (i.e., chemical potential) but, rather, by the thermodynamic factors specific to each material. These findings indicated that while C_{Li} alone could not precisely predict the ease of reaction progression between active materials and LLZTBO, it did allow for a rough classification of reactivity. Consequently, this approach proved useful for the initial screening of material systems suitable for cosintering with LLZTBO.

The high C_{Li} group, including Li_2SnO_3, Li_2TiO_3, and Li_3SbO_4, showed strong chemical stability against LLZTBO cosintering at 850 °C, which could be considered as promising cosintered type anode candidates of garnet-type solid-state electrolyte. To understand the detailed behavior during the sintering process, we investigated the sintering temperature dependence of the reactivity with LLZTBO. The XRD patterns of LLZTBO−Li_2SnO_3 and LLZTBO−Li_2TiO_3 after sintering at various temperatures are shown in Figure 5(a,b). For LLZTBO−Li_2SnO_3 composite samples, no obvious peak change could be observed through the XRD patterns, suggesting that Li_2SnO_3 can be cosintered with LLZTBO, leading to strong chemical stability. Additionally, in the case of the composite LLZTBO−Li_2TiO_3, no obvious peak difference could be observed when sintering from 750 to 900 °C for 5 h. An additional impurity peak appeared when the sintering time was extended from 5 to 15 h at 900 °C; these unknown species might contribute to increased interdiffusion between the anode and electrolyte, as well as the side reaction occurring at the interface, as described in detail later. The same tendency was also confirmed from the results of LLZTBO−Li_3SbO_4 shown in Figure S12.

3.2. Sintering Behavior and Characterization of Composite Pellets. The relative density of the cosintered pellet is significant for designing the all-solid-state battery. Low relative density leads to high electrical resistance related to electronic and ionic conduction, resulting in poor battery performance. Therefore, relative densities of composite LLZTBO−Li_2SnO_3 and LLZTBO-Li_2TiO_3 pellets as a function of the sintering temperature have been measured and shown in Figure 6(a) and (b), respectively. As seen in Figure 6, the relative densities of both LLZTBO−Li_2SnO_3 and LLZTBO-Li_2TiO_3 pellets increased with an increase in the sintering temperature. When further extending the sintering time from 5 to 15 h at 900 °C, the relative densities of LLZTBO−Li_2SnO_3 and LLZTBO-Li_2TiO_3 could achieve as high as 89% and 95%, respectively. In addition, the relative density of LLZTBO-Li_3SbO_4 is shown in Figure S13. These results demonstrated high potential for high C_{Li} materials as the anode materials suitable for cosintering and densification with LLZTBO.

To evaluate the interdiffusion of composite pellets after cosintering, lattice parameter a of cubic LLZTBO ($a = b = c$) and standard data were analyzed by Rietveld refinement in Figure 7. The results of LLZTBO−Li_3SbO_4 are shown in Figure S14. ICSD No. 22957 (crystal structure: cubic $Li_{6.5}La_3Zr_{1.5}Ta_{0.5}O_{12}$, space group: $Ia\bar{3}d$) was used as the initial model. As seen in Figure 7, compared with the cubic LLZTBO, a larger lattice parameter a of LLZTBO after ball-milling could be observed, which originated from the proton exchange that occurred, resulting in the formation of H-substituted LLZTBO. Thereafter, this H-substituted LLZTBO gradually reverted to its original LLZ structure as the sintering temperature increased. It is noted that the lattice parameter after sintering at high temperature strongly depends on the kinds of cosintered electrode materials. When LLZTB is sintered alone or cosintered with Li_2SnO_3, no significant change in lattice parameter is observed. However, cosintering with Li_2TiO_3 and Li_3SbO_4 shows a tendency for the lattice parameter to decrease. Here, the ionic radii of the elements contained in each electrode material follow the order: Sb^{5+} (0.6 Å) < Ti^{4+} (0.605 Å) < Sn^{4+} (0.69 Å) < Zr^{4+} (0.72 Å).[59] Based on the TEM observations discussed later, these elements are likely to undergo mutual diffusion with Zr and become incorporated into the LLZ structure as a solid solution. Therefore, the decrease in the lattice parameter observed during high-temperature sintering, which depends on the type

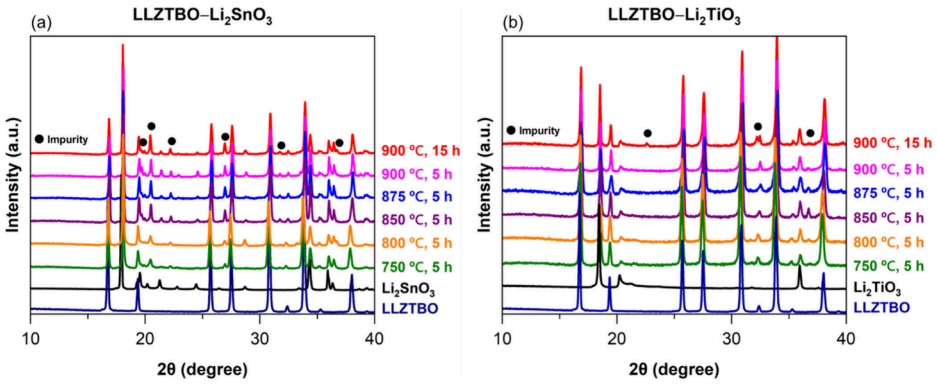

Figure 5. Sintering temperature dependence of (a) LLZTBO−Li_2SnO_3 and (b) LLZTBO−Li_2TiO_3.

https://doi.org/10.1021/acsaem.5c02930
ACS Appl. Energy Mater. 2025, 8, 16964−16973

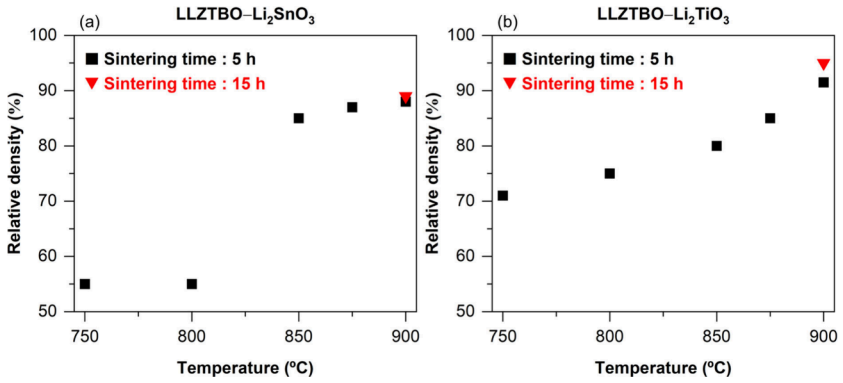

Figure 6. Relative densities of (a) LLZTBO−Li_2SnO_3 and (b) LLZTBO−Li_2TiO_3 as a function of the sintering temperature.

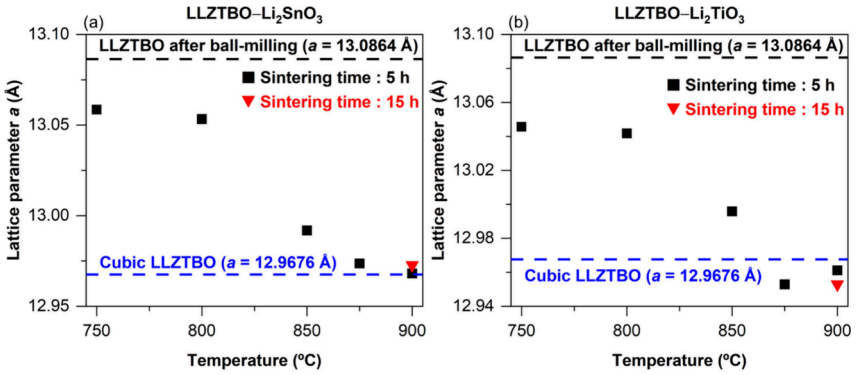

Figure 7. Lattice parameter *a* of LLZTBO in (a) LLZTBO−Li_2SnO_3 and (b) LLZTBO−Li_2TiO_3 as a function of the sintering temperature.

of electrode material, is considered to result from the substitution of smaller ions from the electrode into the LLZ lattice in place of Zr.

Specifically, to reveal the interdiffusion as well as the side reaction occurred at the interface, the enlarged TEM images and element distribution of LLZTBO−Li_2SnO_3 sintering at 900 °C for 15 h were conducted and shown in Figure 8. The overall TEM image and element mappings of LLZTBO−Li_2SnO_3 are shown in Figure S15. The overlap within the Sn-rich parts, the Zr-rich parts, and the La-rich parts showed three different areas: A, B, and C. Mass ratios of each element in these three areas using EDS are summarized in Table 3. According to the results of quantitative analysis, Area A was considered to contain Li_2SnO_3 with a small amount of Zr diffused from LLZTBO. The Sn−Zr−O contained substance in Area B suggested the impurity contributed by the side reaction at the LLZTBO and Li_2SnO_3 interface. Area C matched the La-rich parts, which reflected the LLZTBO with Sn diffused into the Zr sites. TEM results showed that interdiffusion in the composite LLZTBO−Li_2SnO_3 pellet was critical. The generation of such impurities might significantly increase the interfacial resistance, leading to the degradation of battery performance.[60] Therefore, interdiffusion between the anode and LLZTBO should be a priority to consider in the design of the battery. Element substitution into LLZ could be considered a possible approach to achieve interdiffusion suppression.

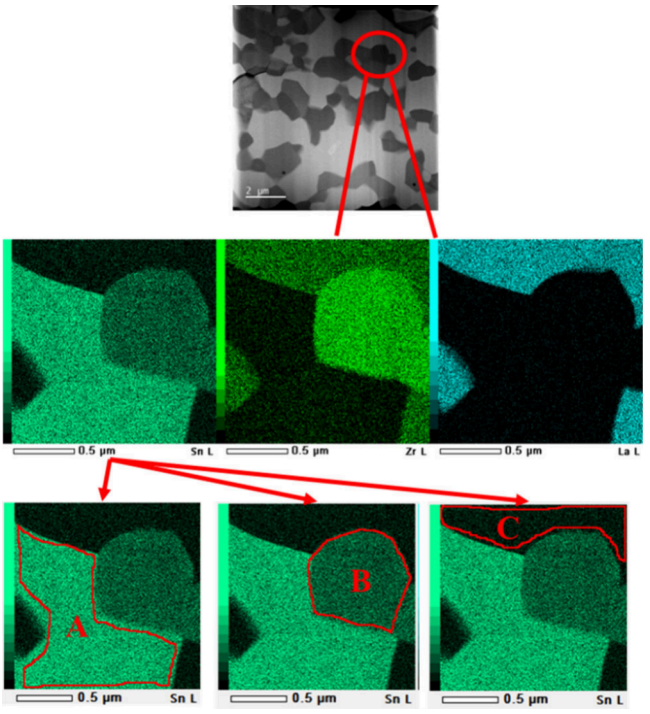

Figure 8. TEM images and elemental mappings of the Sn-rich, Zr-rich, and La-rich parts of LLZTBO−Li_2SnO_3 sintering at 900 °C for 15 h.

3.3. Electrode Performance for Composite Anode Pellets. Finally, to reveal the electrode property for high C_{Li} materials cosintered with LLZTBO, charge−discharge tests of Li | 1 M $LiPF_6$ | LLZTBO-Li_2SnO_3 and Li | 1 M $LiPF_6$ | LLZTBO-Li_2TiO_3 have been carried out at room temperature and shown in Figure 9. As seen in Figure 9(a), a typical reversible charge−discharge curve of Li_2SnO_3 successfully appeared at a constant current density of 134 $\mu A/cm^2$ (0.01C).

https://doi.org/10.1021/acsaem.5c02930
ACS Appl. Energy Mater. 2025, 8, 16964−16973

Table 3. Mass Ratio of Elements in Different Parts

Element	Mass ratio [%]		
	A	B	C
O	26.96	25.32	16.59
Zr	1.78	32.25	12.35
Sn	70.17	40.38	8.12
La	0.28	1.03	51.63
Ta	0.42	0.56	5.07
Bi	0.38	0.45	6.23
Total	100	100	100

A huge drop of the potential at initial discharge (Cycle 1) indicated a significant polarization of the anode due to the poor electrical conductivity of Li_2SnO_3 ($\sim 10^{-9}$ S/cm) as reported;[57] meanwhile, the smooth discharge curve from second cycle was attributed to the formation of Sn-metal,[61] resulting in significant electrical conductivity improvement of anode. Surprisingly, the discharge capacity in the first cycle was around 600 mAh/g. Nevertheless, nearly 250 mAh/g of irreversible discharge capacity appeared at the first delithiation process (the Coulombic efficiency: 63%), which was coming from the formation of the solid electrolyte interface (SEI) and huge volume expansion of Li_2SnO_3. However, Coulombic efficiency at the second cycle was as high as 92% with nearly 600 mAh/g of reversible capacity, which was due to a significant enhancement of electrical conductivity related to the formation of Sn metal.[61] As a reference, the battery performance of the Li_2SnO_3 (via SSR) electrode, composed with acetylene black and PVDF binder, was reported to achieve nearly 400 mAh/g reversible capacity at a current of 60 mA/g, with a capacity fading rate of about 0.4% per cycle.[62] The chemical reaction as well as the lithiation/delithiation process of the Li_2SnO_3 electrode during charge−discharge were written as[62]

$$Li_2SnO_3 + 4Li^+ + 4e^- \rightarrow 3Li_2O + Sn$$

$$Sn + xLi^+ + xe^- \leftrightarrow Li_xSn \quad (x \leq 4.4)$$

Despite the successful proof of composite LLZTBO−Li_2SnO_3 anode used for a liquid electrolyte, the electrode property of LLZTBO−Li_2TiO_3 was at a low level, compared to the theoretical capacity of Li_2TiO_3 (229 mAh/g).[63] As a reference, the Li_2TiO_3 (via SSR) electrode, composed with acetylene black and binder, was reported to achieve nearly 150 mAh/g specific capacity at a current of 100 mA/g, which still exhibits a specific capacity of about 121 mAh/g after 500 cycles.[64] Li_2TiO_3 has been reported as electrochemically inert, and the electrode reaction can be described as below:[64,65]

$$Li_2TiO_3 + xLi^+ + xe^- \leftrightarrow Li_{2+x}TiO_3$$

Such mechanisms indicated that there was no Ti-metal product involved during the insertion/extraction of the Li ion. The same tendency could be observed in LLZTBO−Li_3SbO_4 composite pellets (Figure S16). Additionally, the battery performance of the Li_3SbO_4 electrode, composed with acetylene black and binder, was reported to exhibit a reversible capacity of 81 mAh/g at a current density of 0.05 mA/cm^2 (C/5) and remain unchanged with cycling (after 100 cycles).[66] Contrarily, Sn-metal formation during the charge−discharge test in the LLZTBO-Li_2SnO_3 pellet significantly increases the electronic pathway, resulting in a large discharge capacity and good battery performance. Therefore, it could be speculated that the electronic pathway is limited in LLZTBO−Li_2TiO_3 due to the poor electrical properties of Li_2TiO_3. This results in intercalation and extraction of Li-ion occurring only on the current collector side, leading to poor battery performance. To suppress this, introducing an electrochemically active additive with strong chemical stability against LLZ and anode material into the composite pellet may significantly increase the electronic pathway, resulting in good battery performance.

4. CONCLUSIONS

In this study, we have provided a favorable approach for screening anode candidates applicable to cosintered-type LLZ-based all-solid-state lithium batteries (ASSLBs). Herein, the relationship between lithium concentration (C_{Li}) in the electrode materials and the reactivity of LLZTB has been investigated. The interfacial reaction of cosintered LLZ/Anode at elevated temperature is predictable: high C_{Li} materials (larger than that of LLZ) achieve interaction suppression attributed to the absence of a Li-diffusion driving force, whereas electrodes with lower C_{Li} show weak chemical stability against LLZ due to the occurrence of Li loss in LLZ. In the case of high C_{Li} materials, interdiffusion and side reactions at the interface of the composite LLZ/Anode should be carefully considered. Interdiffusion between the electrolyte and electrode leads to a decrease in the number of active materials. Meanwhile, the generation of impurities may drastically reduce the interfacial resistance, resulting in a poor battery performance. The electrode performance of the cosintered anode using a liquid electrolyte-based half-cell has been investigated. A typical reversible charge−discharge curve of the LLZTBO−

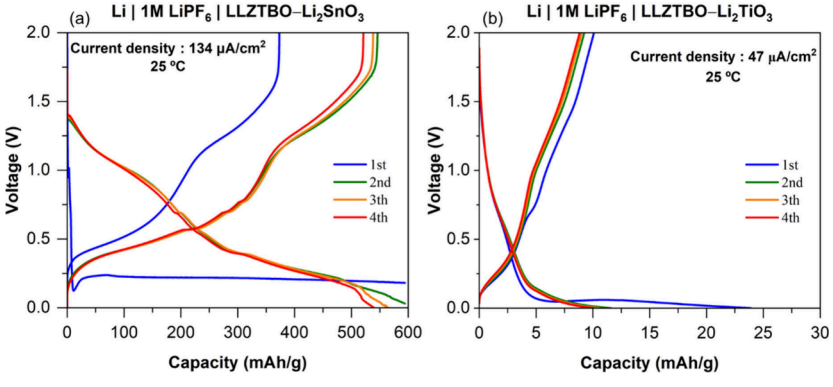

Figure 9. Charge−discharge curves of (a) Li | 1 M $LiPF_6$ | LLZTBO−Li_2SnO_3 and (b) Li | 1 M $LiPF_6$ | LLZTBO−Li_2TiO_3 at room temperature.

https://doi.org/10.1021/acsaem.5c02930
ACS Appl. Energy Mater. 2025, 8, 16964−16973

Li_2SnO_3-based half-cell could be successfully observed, and a reversible capacity of 600 mAh/g with 92% of Coulombic efficiency was achieved. These results demonstrate the effectiveness of the C_{Li}-based materials screening, and we believe that the proposed method can accelerate the development of cosintered ASSLBs based on various electrolytes.

■ ASSOCIATED CONTENT

Supporting Information

The Supporting Information is available free of charge at https://pubs.acs.org/doi/10.1021/acsaem.5c02930.

Synthesis information on anode candidates; XRD patterns of composite materials; sintering dependence, relative densities, lattice parameter, and charge−discharge curves of LLZTBO−Li_3SbO_4 composite disk (PDF)

■ AUTHOR INFORMATION

Corresponding Author

Ken Watanabe − *Department of Advanced Materials Science and Engineering, Faculty of Engineering Sciences, Kyushu University, Kasuga, Fukuoka 816-8580, Japan;* orcid.org/0000-0001-7374-7322; Email: watanabe.ken.331@m.kyushu-u.ac.jp

Authors

Zongqi He − *Interdisciplinary Graduate School of Engineering Sciences, Kyushu University, Kasuga, Fukuoka 816-8580, Japan;* orcid.org/0000-0003-1514-4181

Koichi Suematsu − *Department of Advanced Materials Science and Engineering, Faculty of Engineering Sciences, Kyushu University, Kasuga, Fukuoka 816-8580, Japan;* orcid.org/0000-0002-6170-447X

Kazutaka Mitsuishi − *National Institute for Materials Science, Tsukuba, Ibaraki 305-0047, Japan;* orcid.org/0000-0002-9361-4057

Kengo Shimanoe − *Department of Advanced Materials Science and Engineering, Faculty of Engineering Sciences, Kyushu University, Kasuga, Fukuoka 816-8580, Japan*

Complete contact information is available at: https://pubs.acs.org/10.1021/acsaem.5c02930

Notes

The authors declare no competing financial interest.

■ ACKNOWLEDGMENTS

This study is supported by Japan Science and Technology (JST), K program, Grant number JPMJKP24P1. We would like to thank NIMS battery platform for their support for TEM sample preparation.

■ REFERENCES

(1) Scrosati, B.; Garche, J. Lithium batteries: Status, prospects and future. *J. Power Sources* **2010**, *195* (9), 2419−2430.

(2) Gao, Z.; Sun, H.; Fu, L.; Ye, F.; Zhang, Y.; Luo, W.; Huang, Y. Promises, Challenges, and Recent Progress of Inorganic Solid-State Electrolytes for All-Solid-State Lithium Batteries. *Adv. Mater.* **2018**, *30* (17), No. e1705702.

(3) Famprikis, T.; Canepa, P.; Dawson, J. A.; Islam, M. S.; Masquelier, C. Fundamentals of inorganic solid-state electrolytes for batteries. *Nat. Mater.* **2019**, *18*, 1278−1291.

(4) Ma, Y.; Wan, J.; Yang, Y.; Ye, Y.; Xiao, X.; Boyle, D. T.; Burke, W.; Huang, Z.; Chen, H.; Cui, Y.; Yu, Z.; Oyakhire, S. T.; Cui, Y. Scalable, Ultrathin, and High-Temperature-Resistant Solid Polymer Electrolytes for Energy-Dense Lithium Metal Batteries. *Adv. Energy Mater.* **2022**, *12* (15), No. 2103720.

(5) Liu, Y.; Meng, X.; Wang, Z.; Qiu, J. A Li_2S-based all-solid-state battery with high energy and superior safety. *Sci. Adv.* **2022**, *8* (1), No. eabl8390.

(6) Liu, Y.; Zhang, H.; Jiang, N.; Zhang, W.; Arandiyan, H.; Wang, Z.; Luo, S.; Fang, F.; Sun, H. Porous Co_3O_4@CoO composite nanosheets as improved anodes for lithium-ion batteries. *J. Alloy. Compd.* **2020**, *834*, No. 155030.

(7) Ke, X.; Wang, Y.; Ren, G.; Yuan, C. Towards rational mechanical design of inorganic solid electrolytes for all-solid-state lithium ion batteries. *Energy Storage Materials* **2020**, *26*, 313−324.

(8) Zhang, B.; Tan, R.; Yang, L.; Zheng, J.; Zhang, K.; Mo, S.; Lin, Z.; Pan, F. Mechanisms and properties of ion-transport in inorganic solid electrolytes. *Energy Storage Materials* **2018**, *10*, 139−159.

(9) Thangadurai, V.; Narayanan, S.; Pinzaru, D. Garnet-type solid-state fast Li ion conductors for Li batteries: critical review. *Chem. Soc. Rev.* **2014**, *43* (13), 4714−4727.

(10) Zhang, X.; Liu, T.; Zhang, S.; Huang, X.; Xu, B.; Lin, Y.; Xu, B.; Li, L.; Nan, C. W.; Shen, Y. Synergistic Coupling between $Li_{6.75}La_3Zr_{1.75}Ta0.25O_{12}$ and Poly(vinylidene fluoride) Induces High Ionic Conductivity, Mechanical Strength, and Thermal Stability of Solid Composite Electrolytes. *J. Am. Chem. Soc.* **2017**, *139* (39), 13779−13785.

(11) Arandiyan, H.; S Mofarah, S.; Sorrell, C. C.; Doustkhah, E.; Sajjadi, B.; Hao, D.; Wang, Y.; Sun, H.; Ni, B. J.; Rezaei, M.; Shao, Z.; Maschmeyer, T. Defect engineering of oxide perovskites for catalysis and energy storage: synthesis of chemistry and materials science. *Chem. Soc. Rev.* **2021**, *50* (18), 10116−10211.

(12) Gao, Z.; Sun, H.; Fu, L.; Ye, F.; Zhang, Y.; Luo, W.; Huang, Y. Promises, Challenges, and Recent Progress of Inorganic Solid-State Electrolytes for All-Solid-State Lithium Batteries. *Adv. Mater.* **2018**, *30* (17), No. e1705702.

(13) Fan, H.; Mao, P.; Sun, H.; Wang, Y.; Mofarah, S. S.; Koshy, P.; Arandiyan, H.; Wang, Z.; Liu, Y.; Shao, Z. Recent advances of metal telluride anodes for high-performance lithium/sodium−ion batteries. *Mater. Horiz.* **2022**, *9*, 524−546.

(14) Tadanaga, K.; Egawa, H.; Hayashi, A.; Tatsumisago, M.; Mosa, J.; Aparicio, M.; Duran, A. Preparation of lithium ion conductive Al-doped Li7La3Zr2O12 thin films by a sol−gel process. *J. Power Sources* **2015**, *273*, 844−847.

(15) Liu, Z.; Zheng, F.; Xiong, W.; Li, X.; Yuan, A.; Pang, H. Strategies to improve electrochemical performances of pristine metal-organic frameworks-based electrodes for lithium/sodium-ion batteries. *SmartMat* **2021**, *2* (4), 488−518.

(16) Thangadurai, V.; Narayanan, S.; Pinzaru, D. Garnet-type solid-state fast Li ion conductors for Li batteries: critical review. *Chem. Soc. Rev.* **2014**, *43*, 4714−4727.

(17) Han, F.; Zhu, Y.; He, X.; Mo, Y.; Wang, C. Electrochemical Stability of $Li_{10}GeP_2S_{12}$ and $Li_7La_3Zr_2O_{12}$ Solid Electrolytes. *Adv. Energy Mater.* **2016**, *6* (8), No. 1501590.

(18) Buschmann, H.; Dolle, J.; Berendts, S.; Kuhn, A.; Bottke, P.; Wilkening, M.; Heitjans, P.; Senyshyn, A.; Ehrenberg, H.; Lotnyk, A.; Duppel, V.; Kienle, L.; Janek, J. Structure and dynamics of the fast lithium ion conductor "$Li_7La_3Zr_2O_{12}$". *Phys. Chem. Chem. Phys.* **2011**, *13*, 19378−19392.

(19) Ohta, S.; Kobayashi, T.; Asaoka, T. High lithium ionic conductivity in the garnet-type oxide Li_{7-X} $La_3(Zr_{2-X}, Nb_X)O_{12}$ (X = 0−2). *J. Power Sources* **2011**, *196*, 3342−3345.

(20) Murugan, R.; Thangadurai, V.; Weppner, W. Fast Lithium Ion Conduction in Garnet-Type $Li_7La_3Zr_2O_{12}$. *Angew. Chem., Int. Ed.* **2007**, *46*, 7778−7781.

(21) Geiger, C. A.; Alekseev, E.; Lazic, B.; Fisch, M.; Armbruster, T.; Langner, R.; Fechtelkord, M.; Kim, N.; Pettke, T.; Weppner, W. Crystal Chemistry and Stability of "$Li_7La_3Zr_2O_{12}$" Garnet: A Fast Lithium-Ion Conductor. *Inorg. Chem.* **2011**, *50* (3), 1089−1097.

(22) Wolfenstine, J.; Ratchford, J.; Rangasamy, E.; Sakamoto, J.; Allen, J. L. Synthesis and high Li-ion conductivity of Ga-stabilized cubic $Li_7La_3Zr_2O_{12}$. *Mater. Chem. Phys.* **2012**, *134* (2−3), 571−575.
(23) Wagner, R.; Redhammer, G. J.; Rettenwander, D.; Senyshyn, A.; Schmidt, W.; Wilkening, M.; Amthauer, G. Crystal Structure of Garnet-Related Li-Ion Conductor $Li_{7-3x}Ga_xLa_3Zr_2O_{12}$: Fast Li-Ion Conduction Caused by a Different Cubic Modification? *Chem. Mater.* **2016**, *28* (6), 1861−1871.
(24) Rangasamy, E.; Wolfenstine, J.; Sakamoto, J. The role of Al and Li concentration on the formation of cubic garnet solid electrolyte of nominal composition $Li_7La_3Zr_2O_{12}$. *Solid State Ionics* **2012**, *206*, 28−32.
(25) Matsuda, Y.; Sakamoto, K.; Matsui, M.; Yamamoto, O.; Takeda, Y.; Imanishi, N. Phase formation of a garnet-type lithium-ion conductor $Li_{7-3x}Al_xLa_3Zr_2O_{12}$. *Solid State Ionics* **2015**, *277*, 23−29.
(26) Hu, S.; Li, Y.-F.; Yang, R.; Yang, Z.; Wang, L. Structure and ionic conductivity of $Li_7La_3Zr_{2-x}Ge_xO_{12}$ garnet-like solid electrolyte for all solid state lithium ion batteries. *Ceram. Int.* **2018**, *44* (6), 6614−6618.
(27) Brugge, R. H.; Kilner, J. A.; Aguadero, A. Germanium as a donor dopant in garnet electrolytes. *Solid State Ionics* **2019**, *337*, 154−160.
(28) Janani, N.; Ramakumar, S.; Kannan, S.; Murugan, R. Optimization of Lithium Content and Sintering Aid for Maximized Li+ Conductivity and Density in Ta-Doped $Li_7La_3Zr_2O_{12}$. *J. Am. Chem. Soc.* **2015**, *98* (7), 2039−2046.
(29) Hamao, N.; Kataoka, K.; Kijima, N.; Akimoto, J. Synthesis, crystal structure and conductive properties of garnet-type lithium ion conductor Al-free $Li_{7-x}La_3Zr_{2-x}Ta_xO_{12}$ ($0 \le x \le 0.6$). *J. Ceram. Soc. Jpn.* **2016**, *124* (6), 678−683.
(30) Ohta, S.; Kobayashi, T.; Asaoka, T. High lithium ionic conductivity in the garnet-type oxide Li_{7-X} $La_3(Zr_{2-X}, Nb_X)O_{12}$ (X = 0−2). *J. Power Sources* **2011**, *196*, 3342−3345.
(31) Song, S.; Chen, B.; Ruan, Y.; Sun, J.; Yu, L.; Wang, Y.; Thokchom, J. Gd-doped $Li_7La_3Zr_2O_{12}$ garnet-type solid electrolytes for all-solid-state Li-Ion batteries. *Electrochim. Acta* **2018**, *270*, 501−508.
(32) Indu, M. S.; Alexander, G. V.; Deviannapoorani, C.; Murugan, R. Realization of room temperature lithium metal battery with high Li^+ conductive lithium garnet solid electrolyte. *Ceram. Int.* **2019**, *45* (17), 22610−22616.
(33) Ramakumar, S.; Satyanarayana, L.; Manorama, S. V.; Murugan, R. Structure and Li^+ dynamics of Sb-doped $Li_7La_3Zr_2O_{12}$ fast lithium ion conductors. *Phys. Chem. Chem. Phys.* **2013**, *15* (27), 11327−11338.
(34) Wagner, R.; Rettenwander, D.; Redhammer, G. J.; Tippelt, G.; Sabathi, G.; Musso, M. E.; Stanje, B.; Wilkening, M.; Suard, E.; Amthauer, G. Synthesis, Crystal Structure, and Stability of Cubic $Li_{7-x}La_3Zr_{2-x}Bi_xO_{12}$. *Inorg. Chem.* **2016**, *55* (23), 12211−12219.
(35) Schwanz, D. K.; Villa, A.; Balasubramanian, M.; Helfrecht, B.; Marinero, E. E. Bi aliovalent substitution in $Li_7La_3Zr_2O_{12}$ garnets: Structural and ionic conductivity effects. *AIP Adv.* **2020**, *10*, No. 03520.
(36) Rettenwander, D.; Welzl, A.; Cheng, L.; Fleig, J.; Musso, M.; Suard, E.; Doeff, M. M.; Redhammer, G. J.; Amthauer, G. Synthesis, Crystal Chemistry, and Electrochemical Properties of $Li_{7-2x}La_3Zr_{2-x}Mo_xO_{12}$ (x = 0.1−0.4): Stabilization of the Cubic Garnet Polymorph via Substitution of Zr^{4+} by Mo^{6+}. *Inorg. Chem.* **2015**, *54* (21), 10440−10449.
(37) Dong, B.; Yeandel, S. R.; Goddard, P.; Slater, P. R. Combined Experimental and Computational Study of Ce-Doped $La_3Zr_2Li_7O_{12}$ Garnet Solid-State Electrolyte. *Chem. Mater.* **2020**, *32* (1), 215−223.
(38) Park, K.; Yu, B. C.; Jung, J. W.; Li, Y.; Zhou, W.; Gao, H.; Son, S.; Goodenough, J. B. Electrochemical Nature of the Cathode Interface for a Solid-State Lithium-Ion Battery: Interface between $LiCoO_2$ and Garnet- $Li_7La_3Zr_2O_{12}$. *Chem. Mater.* **2016**, *28* (21), 8051−8059.
(39) Kim, K. H.; Iriyama, Y.; Yamamoto, K.; Kumazaki, S.; Asaka, T.; Tanabe, K.; Fisher, C. A. J.; Hirayama, T.; Murugan, R.; Ogumi, Z. Characterization of the interface between $LiCoO_2$ and $Li_7La_3Zr_2O_{12}$ in an all-solid-state rechargeable lithium battery. *J. Power Sources* **2011**, *196* (2), 764−767.
(40) Wakasugi, J.; Munakata, H.; Kanamura, K. Thermal Stability of Various Cathode Materials against $Li_{6.25}Al_{0.25}La_3Zr_2O_{12}$ Electrolyte. *Electrochemistry* **2017**, *85* (2), 77−81.
(41) Vardar, G.; Bowman, W. J.; Lu, Q.; Wang, J.; Chater, R. J.; Aguadero, A.; Seibert, R.; Terry, J.; Hunt, A.; Waluyo, I.; Fong, D. D.; Jarry, A.; Crumlin, E. J.; Hellstrom, S. L.; Chiang, Y.-M.; Yildiz, B. Structure, Chemistry, and Charge Transfer Resistance of the Interface between $Li_7La_3Zr_2O_{12}$ Electrolyte and $LiCoO_2$ Cathode. *Chem. Mater.* **2018**, *30* (18), 6259−6276.
(42) Kato, T.; Hamanaka, T.; Yamamoto, K.; Hirayama, T.; Sagane, F.; Motoyama, M.; Iriyama, Y. In-situ $Li_7La_3Zr_2O_{12}/LiCoO_2$ interface modification for advanced all-solid-state battery. *J. Power Sources* **2014**, *260*, 292−298.
(43) Ren, Y.; Liu, T.; Shen, Y.; Lin, Y.; Nan, C.-W. Chemical compatibility between garnet-like solid state electrolyte $Li_{6.75}La_3Zr_{1.75}Ta_{0.25}O_{12}$ and major commercial lithium battery cathode materials. *J. Materiomics* **2016**, *2* (3), 256−264.
(44) Akimoto, J.; Akao, T.; Nagai, H.; Kataoka, K. Low-Temperature Sintering of a Garnet-Type $Li_{6.5}La_3Zr_{1.5}Ta_{0.5}O_{12}$ Solid Electrolyte and an All-Solid-State Lithium-Ion BatteryClick to copy article link. *ACS Appl. Mater. Interfaces* **2023**, *15* (15), 18973−18981.
(45) Akimoto, J.; Akao, T.; Kataoka, K. Low-Temperature Fabrication of Bulk-Type All-Solid-State Lithium-Ion Battery Utilizing Nanosized Garnet Solid Electrolytes. *Small* **2023**, *19* (40), No. 2301617.
(46) Ichihara, F.; Miyoshi, S.; Ode, M.; Masuda, T. Co-sintering Reaction Analysis of LiCoO2 Cathodes and NASICON-Type LATP Solid Electrolytes Studied by Experimental and Computational Methods. *J. Phys. Chem. C* **2025**, *129* (28), 12738−12749.
(47) Watanabe, K.; Tashiro, A.; Ichinose, Y.; Takeno, S.; Suematsu, K.; Mitsuishi, K.; Shimanoe, K. Lowering the sintering temperature of $Li_7La_3Zr_2O_{12}$ electrolyte for co-fired all-solid-state batteries via partial Bi substitution and precise control of compositional deviation. *J. Ceram. Soc. Jpn.* **2022**, *130* (7), 416−423.
(48) Hayashi, N.; Watanabe, K.; Shimanoe, K. Low-temperature sintering characteristics and electrical properties of Ca- and Bi-doped $Li_7La_3Zr_2O_{12}$ electrolyte containing Li_3BO_3 additive. *J. Mater. Chem. A* **2023**, *11* (4), 2042−2053.
(49) Hayashi, N.; Watanabe, K.; Ohnishi, T.; Takada, K.; Shimanoe, K. Impact of intentional composition tuning on the sintering properties of Ca−Bi co-doped $Li_7La_3Zr_2O_{12}$ for co-fired solid-state batteries. *J. Mater. Chem. A* **2023**, *11* (29), 15681−15690.
(50) Hayashi, N.; Watanabe, K.; Shimanoe, K. Co-sintering a cathode material and garnet electrolyte to develop a bulk-type solid-state Li metal battery with wide electrochemical windows. *J. Mater. Chem. A* **2024**, *12* (9), 5269−5281.
(51) Mukhopadhyay, A.; Jangid, M. K. Li metal battery, heal thyself. *Science* **2018**, *359* (6383), 1463.
(52) Sharafi, A.; Meyer, H. M.; Nanda, J.; Wolfenstine, J.; Sakamoto, J. Characterizing the Li−$Li_7La_3Zr_2O_{12}$ interface stability and kinetics as a function of temperature and current density. *J. Power Sources* **2016**, *302*, 135−139.
(53) Ma, C.; Cheng, Y.; Yin, K.; Luo, J.; Sharafi, A.; Sakamoto, J.; Li, J.; More, K. L.; Dudney, N. J.; Chi, M. Interfacial Stability of Li Metal-Solid Electrolyte Elucidated via in Situ Electron Microscopy. *Nano Lett.* **2016**, *16* (11), 7030−7036.
(54) Wu, B.; Wang, S.; Evans, W. J., IV; Deng, D. Z.; Yang, J.; Xiao, J. Interfacial behaviours between lithium ion conductors and electrode materials in various battery systems. *J. Mater. Chem.* **2016**, *4* (40), 15266−15280.
(55) Ohnishi, T.; Sakaguchi, I.; Takada, K. Surface Treatment of Garnet-Type Solid Electrolyte for Suppressing Dendritic Growth. *ACS Appl. Energy Mater.* **2024**, *7* (13), 5321−5325.
(56) Zhao, Q.; Ma, L.; Zhang, Q.; Wang, C.; Xu, X. SnO_2-Based Nanomaterials: Synthesis and Application in Lithium-Ion Batteries and Supercapacitors. *J. Nanomater.* **2015**, *2015*, 1−15.

https://doi.org/10.1021/acsaem.5c02930
ACS Appl. Energy Mater. 2025, 8, 16964−16973

(57) Kamali, A. R.; Fray, D. J. Tin-based materials as advanced anode materials for lithium ion batteries: a review. *Rev. Adv. Mater. Sci.* **2011**, *27*, 14−24.
(58) Hamao, N.; Hamamoto, K.; Taguchi, N.; Tanaka, S.; Akimoto, J. Synthesis and crystal structure of fluorite-type $La_{2.4}Zr_{1.2}Ta_{0.4}O_7$: A precursor oxide for low temperature formation of garnet-type $Li_{6.5}La_3Zr_{1.5}Ta_{0.5}O_{12}$. *Solid State Ionics* **2020**, *357*, No. 115460.
(59) Shannon, R. D. Revised Effective Ionic Radii and Systematic Studies of Interatomie Distances in Halides and Chaleogenides. *Acta Crystallogr.* **1976**, *A32*, 751−767.
(60) Maruno, M.; Nakayama, F.; Suzuki, Y.; Sakakura, M.; Ohnishi, T.; Nomura, Y.; Hiraoka, K.; Yamamoto, K.; Yajima, T.; Iriyama, Y. Chemical design rules for low-resistivity electrode−electrolyte interfaces in all-solid-state lithium batteries. *Commun. Mater.* **2025**, *6*, (144), DOI: 10.1038/s43246-025-00870-8.
(61) Wang, K.; Joshi, Y.; Chen, H.; Schmitz, G. In-situ analysis of solid-electrolyte interphase formation and cycle behavior of Sn battery anodes. *J. Power Sources* **2022**, *535*, No. 231439.
(62) Zhang, D.W.; Zhang, S.Q.; Jin, Y.; Yi, T.H.; Xie, S.; Chen, C.H. Li_2SnO_3 derived secondary Li−Sn alloy electrode for lithium-ion batteries. *J. Alloy. Compd.* **2006**, *415* (1−2), 229−233.
(63) Lakshmi-Narayana, A.; Dhananjaya, M.; Guru-Prakash, N.; Hussain, O. M.; Mauger, A.; Julien, C. M. Li_2TiO_3/Graphene and Li_2TiO_3/CNT Composites as Anodes for High Power Li−Ion Batteries. *Chemistry Select* **2018**, *3* (31), 9150−9158.
(64) Xie, Y.; Wang, Q.; Gu, F.; Dai, K.; Shui, M.; Shu, J. The electrochemical properties and intercalation mechanism of low strain Li_2TiO_3 as a high-performance anode material for lithium-ion batteries. *J. Alloy. Compd.* **2022**, *893*, No. 162348.
(65) Lu, J.; Peng, Q.; Wang, W.; Nan, C.; Li, L.; Li, Y. Nanoscale Coating of $LiMO_2$ (M = Ni, Co, Mn) Nanobelts with Li^+-Conductive Li_2TiO_3: Toward Better Rate Capabilities for Li-Ion Batteries. *J. Am. Chem. Soc.* **2013**, *135* (5), 1649−1652.
(66) Kundu, M.; Mahanty, S.; Basu, R. N. Li_3SbO_4: A new high rate anode material for lithium-ion batteries. *Mater. Lett.* **2011**, *65* (7), 1105−1107.

https://doi.org/10.1021/acsaem.5c02930
ACS Appl. Energy Mater. 2025, 8, 16964−16973